



LAWRENCE
LIVERMORE
NATIONAL
LABORATORY

Godiva and Juliet Diagnostics CED-1 (IER-176)

J. C. Scorby

December 23, 2011

Disclaimer

This document was prepared as an account of work sponsored by an agency of the United States government. Neither the United States government nor Lawrence Livermore National Security, LLC, nor any of their employees makes any warranty, expressed or implied, or assumes any legal liability or responsibility for the accuracy, completeness, or usefulness of any information, apparatus, product, or process disclosed, or represents that its use would not infringe privately owned rights. Reference herein to any specific commercial product, process, or service by trade name, trademark, manufacturer, or otherwise does not necessarily constitute or imply its endorsement, recommendation, or favoring by the United States government or Lawrence Livermore National Security, LLC. The views and opinions of authors expressed herein do not necessarily state or reflect those of the United States government or Lawrence Livermore National Security, LLC, and shall not be used for advertising or product endorsement purposes.

This work performed under the auspices of the U.S. Department of Energy by Lawrence Livermore National Laboratory under Contract DE-AC52-07NA27344.

Introduction

A suite of diagnostics are being proposed for use in the Juliet experiment (IER-128). In order to calibrate and test the diagnostics prior to use, the LLNL calibration facility and Godiva pulsed reactor will be used to provide intense sources of neutrons and gammas. Due to the similarities of the Godiva and Juliet radiation fields, the diagnostics being developed and tested for Juliet can also play an on-going role in diagnostics for Godiva as well as, perhaps, other critical assembly experiments. Similar work is also being conducted for IER-147 for the purpose of characterizing the Godiva radiation field in support of an upcoming international nuclear accident dosimetry exercise. Diagnostics developed and fielded under IER-147 can provide valuable data with respect to the neutron and gamma energy spectrums in the vicinity of Godiva which is relevant to the calibration of Juliet diagnostics.

Collaborations

LANL and LLNL have strong diagnostics groups supporting NIF, non-proliferation, UGTs, subcrits, etc. Expertise from these groups has been sought in the selection of diagnostics and some collaborations have been established. The LLNL Test Readiness Program has offered to field and analyze data from the Alpha Box scintillator/PD/PMT system, neutron trap, and vacuum Compton diodes (see table below). They will also provide activation foils and some measurement services for characterizing the room environment in the vicinity of Godiva. The LLNL Advanced Detector Design Group is providing assistance in the design and testing of a neutron time of flight spectrometer and LLNL Radiochemistry and Dosimetry groups will support fielding and measurements of activation and radchem foils. The collaborations help the Juliet experiment and also provide maintenance of or re-generation of diagnostic capabilities at LLNL needed for other programs.

Diagnostics Development and Testing Plan

The diagnostics schedule spans FY12 and FY13. Testing of diagnostics will fall under two campaigns. Primary diagnostics are those considered to provide the highest probability of success and are ready or near ready-to-deploy commercial or LLNL assets. The development and testing of these diagnostics will occur in FY12 with results reported by the end of the fiscal year. Additional diagnostics, designated as secondary, will be tested during FY13. The complete schedule of milestones and deliverables is included in the NCSP 5-yr. Plan.

Some diagnostics cannot be tested as they will be used prior to actual deployment for Juliet. These include diagnostics internal to the assembly: micro-fission meters, thermocouples and RTDs. However, testing external to Godiva and/or within the glory hole, as well as past usage of thermocouples and RTDs, can establish their viability for expected Juliet radiation and temperature fields.

An initial set of calibration measurements will be made to characterize the room environment. These measurements support both IER-147 and this IER-176. The measurements will allow a determination of the neutron energy spectrum in the room based on a “clean” ^{252}Cf source. This data is necessary to properly calibrate foils and detector responses expected for Godiva and Juliet. These measurements need to be performed prior to Godiva re-assembly. Refer to CED-1 for IER-147 for details of the detectors, their sensitivities and expected accuracies.

Pending approval of CED-1, LLNL will proceed to final design CED-2. The following actions will need to be taken for CED-2:

- Preparation of all documents needed for procurements, instrument loan agreements, and agreements for collaborative work
- Development of a comprehensive LLNL test plan
- Identification of applicable NSTec and Laboratory requirements for performing work with diagnostic equipment within the NCERC
- Qualification of LLNL personnel and collaborators
- Identification of all necessary elements of NSTec “work packages” to enable introduction of LLNL equipment to the DAF, installation within NCERC, utilization by LLNL personnel and collaborators, handling of radioactive materials, return of equipment to LLNL
- Identification of any necessary changes to Laboratory Secondary Real Estate Operating Permits
- Identification and starting work on resolving any authorization basis issues

Upon approval of final design, LLNL will complete the items described above during the initial experiment execution initiation phase (CED-3a), and deploy all necessary equipment to the NNSS.

Project Risks and Risk Management

Budget limitations at other laboratories may preclude their ability to participate in the actual experiments within NCERC. Instrument loans may not be possible from other laboratories or LLNL organizations due to schedule conflicts requiring their use at the home organization during the time experiments are scheduled at NCERC. Schedule delays may occur during Godiva-IV reassembly complicating schedule planning.

Budget limitations for this task preclude full transfer of measurement responsibilities to collaborating organizations unless there is cost sharing. If other organizations were unable to share the cost burden, a smaller suite of diagnostics would need to be deployed. Use of existing ready-to-deploy assets from other organizations, with minimal start-up requirements, best avoids these risks. LLNL is negotiating cost sharing to provide the best collaborative framework possible based on funding.

Diagnostics Suite

The following table includes all the diagnostics under consideration for Juliet. Not all the diagnostics in the table will end up being tested or fielded due to budget and schedule constraints and the expected success of primary or secondary diagnostics. Those which are considered as primary diagnostics to be tested in FY12 are marked with a “P” in the table. Secondary diagnostics are marked with an “S” for potential testing in FY13.

Diagnostics		
Type and Designation	Description	Measured Quantity
Internal to Assembly		
MICRO-FMS P	Micro-fission chambers inserted in core at 0.2, 0.5, and 0.8 L.	Current rate vs. time corresponding to local neutron flux at detector location.
FIBER OPTIC	Fiber optic cables with pre-drilled holes inserted in core at 0.2 and 0.8 L in a spiral radial configuration.	Light pulses corresponding to shock arrival times at each hole.
FIBER OPTIC	Fiber optic cable wound radially around core in gap at 0.8 L	Changes in interference pattern as a function of time corresponding to surface outward velocity as a function of time.
ACTIVATION AND RADCHEM FOILS	Activation foils located at internal points. Various foil materials, no shielding.	Neutron induced radioactivity corresponding to integrated neutron flux at foil location.
THERMOCOUPLES RTDS	“Intrinsic” thermocouples and RTDs located at several internal points.	Current rate vs. time corresponding to temperature at the thermocouple/RTD location.
LIF	Laser induced fluorescence of flour added to surface, pinhole FO into assembly	Change in decay rate of induced fluorescence corresponding to surface temperature.

Type and Designation	Description	Measured Quantity
External to Assembly		
COMPTON DIODES S	Compton diode, collimated view, multiple gains.	Current rate vs. time corresponding to ^{238}U photo fissions induced by gammas. Fission rate linear with gamma emission rate. Variable gains to allow many decades of flux detection.
n/ γ CONVERTOR	BC403 scintillator plate +PMT, collimated, direct 90° convertor plate view.	Scintillator light output vs. time corresponding to neutron emission rate. Neutrons converted to gammas by Al convertor plate
CVD Diamond P	CVD Diamond solid state array, collimated, shielded view, multiple gains.	Current rate vs. time corresponding to assembly neutron and gamma emission rates. Neutron/gamma signals separated by voltage. Variable gains to allow many decades of flux detection.
PROTON RECOIL S	Proton/a-Si recoil PIN diode. Collimated, shielded view.	Current rate vs. time corresponding to assembly neutron emission rate at the detector axial position.
Si PLATE	Si plate + PCM, shielded pinhole view.	PCM charge vs. time per pixel corresponding to neutron spatial emission rate.
SCINTILLATOR (ALPHA BOX) P	BC403 scintillator cube viewed by 4 detectors (PMTs and/or PDs)	Scintillator light vs. time corresponding to neutron and gamma spatial emission rates.
NEUTRON TRAP P	Large BC403 scintillator cube viewed by PMT, time gated	Scintillator light from proton capture gammas after long time gate corresponding to total neutron yield.
TOF S	Thin liquid scintillator, evacuated flight path, and larger plastic scintillator provide timing signals of individual neutron scattering and capture in scintillators.	Flight time between detector elements provides precise neutron energy determination of individual neutrons.
IONIZATION TUBE S	^3He is ionized by neutrons in a high-pressure tube. Ions are collected on anode.	Current of anode corresponding to neutron flux at tube.
CR-39 PACK P	CR-39 film pack, shielded pinhole view.	Etched holes in film corresponding to integrated neutron yield.

Type and Designation	Description	Measured Quantity
ACTIVATION AND RADCHEM FOILS P	Activation foils located exterior to assembly at various locations. Various foil materials and shields.	Neutron induced radioactivity corresponding to integrated neutron flux at foil location. Foil shields and sandwiching provide some spectral information.
PDV/VISAR S	VISAR/PDV system FO directed on outside surface of assembly	Changes in interference pattern as a function of time corresponding to surface outward velocity as a function of time.
PINSHORTS	Shorting pin set located at 0.2L.	Time progression of pin shorts corresponding to the arrival time of the outer metal surface of assembly at the pins.
RFS S	Retroreflective shadowgraphy system with high-speed camera.	Time variations in image distortions on reflective screen caused by index changes in air due to shock propagation. Large movements of assembly can also be photographed.

Description of Primary and Secondary Diagnostics

Compton Diodes

Fission gammas can be detected by measuring the electron current generated by Compton scattering in a target. Proper selection of entrance and exit window, and cathode materials can be used to optimize the detection of 1 – 3 MeV gammas consistent with the energy spectrum of fission gammas. A schematic of such a device is provided below.

Sensitivity: < 1 ns response time with typically $5 \times 10^{-3} \text{ e}^-/\text{MeV}$

Dynamic Range: Up to 100 A with linear response

Advantages

- Useable in high flux conditions (max flux of $10^{23} \text{ MeV}/\text{cm}^2\text{sec}$)
- Large dynamic range
- Sensitivity roughly flat over fission gamma energy spectrum.

Disadvantages

- No energy spectrum information
- Very Low sensitivity applicable to only the peak fluxes

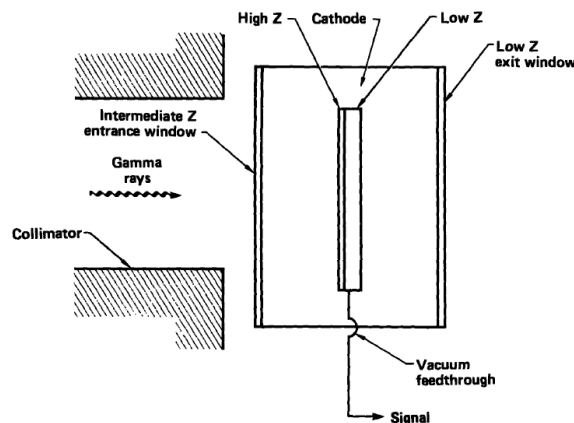


Figure 13. A cylindrical Compton diode whose material and thickness are chosen to optimize sensitivity in the 1- to 3-MeV energy range. This detector is designed to operate in a collimated gamma-ray beam.

Proton Recoil

Neutrons can be measured by detection of recoil protons by a PIN diode. A thin poly sheet is placed in the neutron flux path as the target. Recoil protons are generated by neutron elastic scattering off the hydrogen in the poly. The protons are detected by a PIN diode which is located out of the neutron flux path to reduce background. A Faraday cup can also be used to collect protons if less sensitivity is necessary. The angle between the path of the recoil protons and the incident neutron flux should be kept small to maximize the differential scattering cross section which varies as the cosine of the angle and the proton energy which varies as the square of the cosine.

A schematic of the detector is provided below (Ebert 1986). The recoil proton flight path must be kept at vacuum and a thin Al ranging filter can be placed at the PIN diode to remove scattered electron background as well as lower energy protons. With regard to that function, the detector sensitivity can be tuned to only the higher energy tail of the fission spectrum thereby reducing some of flight time dispersion. Another variant of the proton recoil type detector is discussed by Ouyang (NIM A, 481, 2002) where the proton converter, absorber, detector, and insulating layers are all sandwiched together for direct-on neutron measurement in high flux pulsed reactor applications.

Similarly, an a-Si disk can be used as the neutron target. In this case, neutron captures on Si produce alpha and deuteron charged particles which can be detected by the PIN diode. The appropriate angle for off-axis detection will need to be determined.

Sensitivity: 3 - 5 ns response time

Dynamic Range: 3 - 10 A with linear response

Advantages

- Useable in high flux conditions
- Large dynamic range
- May be located close to assembly to minimize time dispersion.

Disadvantages

- Low sensitivity due to ranging filter and angled flight path. May be susceptible to high relative background.

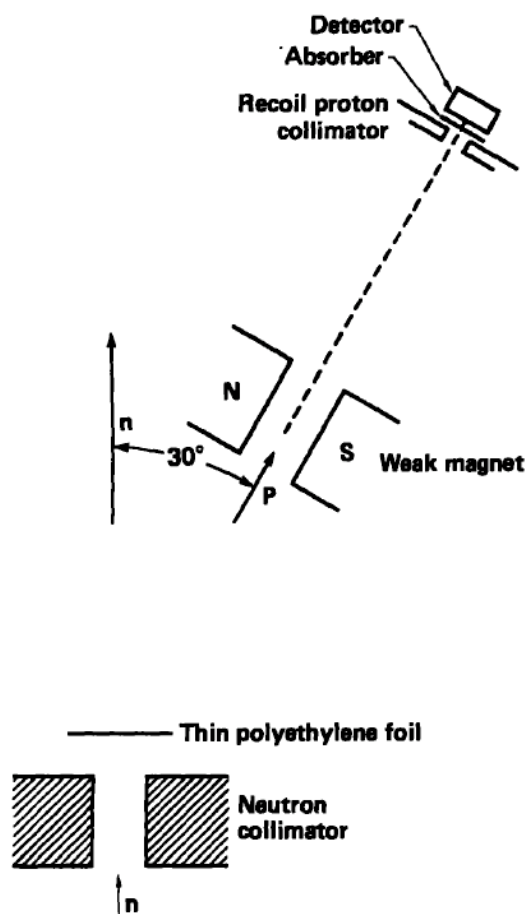


Figure 7. Schematic diagram of a recoil proton detector. The collimated neutrons collide elastically with protons in the polyethylene. Protons scattered at 30° are detected with a silicon (Si) detector that is shielded from light and low-energy charged particles by a very thin absorber and a weak magnetic field, respectively.

Micro-FMs

Fission chambers have long been used for measurement of neutron flux in nuclear reactors and more recently in fusion reactors. Recent developments in miniature “micro-fission” chambers by KSU (McGregor 2005) are of particular interest. Given their small size ($\sim 2\text{cm}$ across by $\sim \text{few mm}$ deep) it is possible to directly insert several into the fissile core of the experiment without significant perturbation to the fission density and flux. They are insensitive to gammas and able to operate in high flux environments. However, current prototypes have dead times of about 25% for neutron fluxes of $5 \times 10^{12} \text{ n/cm}^2\text{sec}$ when operating in pulse mode. Extension to higher fluxes could perhaps be done by operating in current mode, using a lower density of active fissile material, and a higher threshold energy fission isotope.

A diagram of the KSU micro-fission chamber is provided below as well as a measured output of one such device in the KSU reactor pool.

Sensitivity: Dependent on gas pressure and fissile density on active coated surfaces

Dynamic Range: in excess of $5 \times 10^{12} \text{ n/cm}^2\text{sec}$

Advantages

- Usable in high flux conditions (current mode in fluxes exceeding 10^{12} n/cm^2)
- No noticeable performance degradation for fluences exceeding 10^{19} n/cm^2
- Insensitive to gammas
- Provides temporal and spatial data.

Disadvantages

- Use in fluxes in excess of $5 \times 10^{12} \text{ n/cm}^2\text{sec}$ has not been demonstrated.

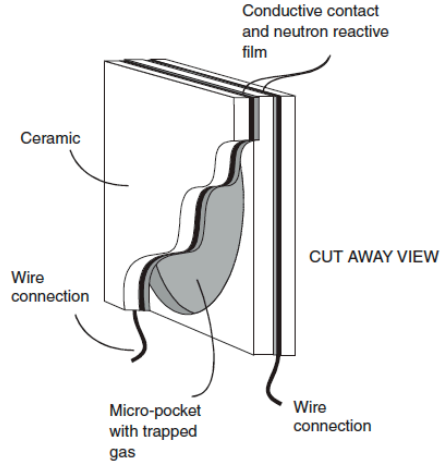


Fig. 1. The micro-pocket fission detector (MPFD) is formed from insulating materials, such as aluminum oxide or oxidized silicon wafers. The opposing sides of each pocket are coated with a conductor followed by a neutron reactive film, such as ^{10}B , ^6LiF , ^{235}U , or ^{232}Th .

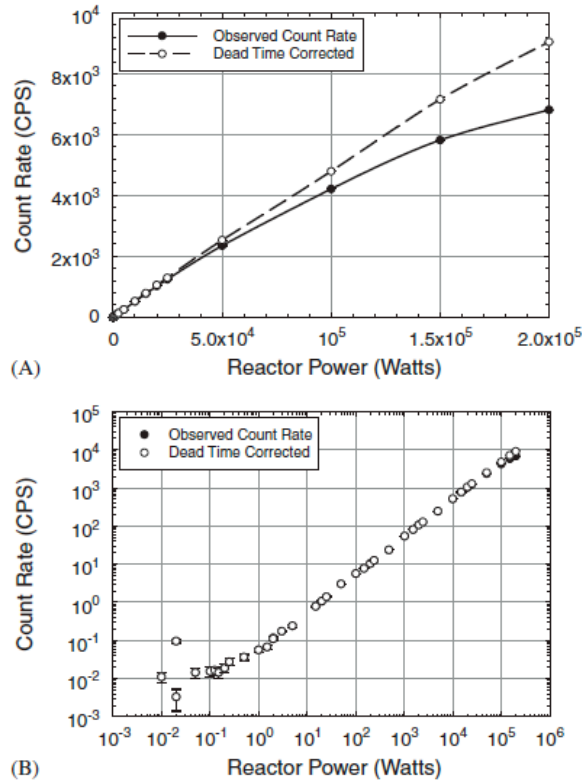


Fig. 7. The above figures show the response of a 3-mm diameter, 1-mm wide MPFD as a function of reactor power as inserted into the center of a 250 kW TRIGA Mark II nuclear reactor, where (A) is a linear plot and (B) is a log-log plot. The most recent devices are only 1 mm in diameter, and are expected to perform with no appreciable deadtime losses with the TRIGA reactor at full power ($\phi_{\text{th}} > 10^{13}$ neutrons $\text{cm}^{-2} \text{s}^{-1}$).

CVD Diamond

Schmidt (Rev. Sci. Instrum., 74, 2003) reports testing of several CVD diamond detectors at OMEGA. The response for “optical grade” CVD diamond to 2.45 MeV neutrons from DD fusion is provided below. CVD diamond detectors will be used at NIF for the highest expected neutron yields of $10^{15} - 10^{19}$. It has been reported (Almaviva 2009) that high neutron fluxes in excess of 10^{16} n/cm²sec causes degradation of CVD diamond detectors. Shielding could be used to reduce the neutron flux at the detectors if necessary to remain well within established operating conditions.

Temporal: 400 ps FWHM. Peak locatable to better than 100 ps

Sensitivity: 0.26 μ V ns/n

Advantages

- Usable in high flux conditions
- Fast temporal response
- Large dynamic range
- Insensitive to gammas and radiation hard

Disadvantages

- Low detection efficiency
(Though diamond has highest detection efficiency theoretically, efficiency is greatly limited by the thickness of the diamond wafer (1 mm) which can be manufactured).

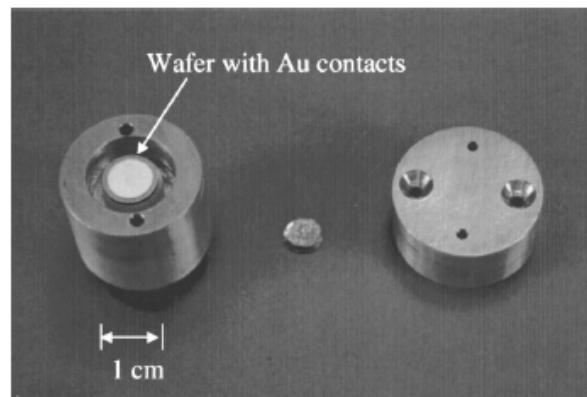


FIG. 2. Disassembled CVD diamond detector. The CVD diamond wafer sits in the Cu housing on left. The Au contact on the bottom of the wafer connects to the central pin of the SMA connector. To seal the assembly, Cu top (right) bolts to body of housing (left). This grounds the top Au contact.

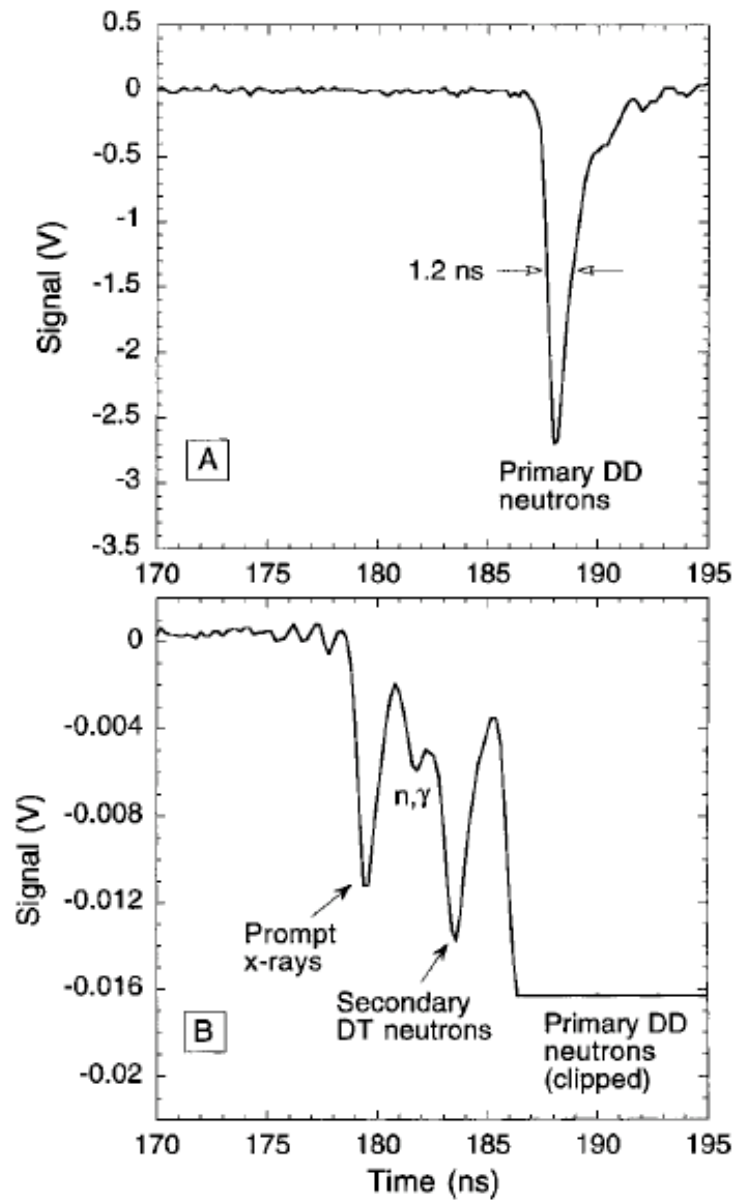


FIG. 4. Response of CVD diamond detector to OMEGA shot 27449 (D2 fuel). The signal was split into two scope channels, A and B. Channel B, with the expanded vertical axis, sends the primary signal off-scale. The total neutron yield for this shot was 1.62×10^{11} . The detector was at 16 cm from magnet chamber center.

Scintillator - Alpha Box

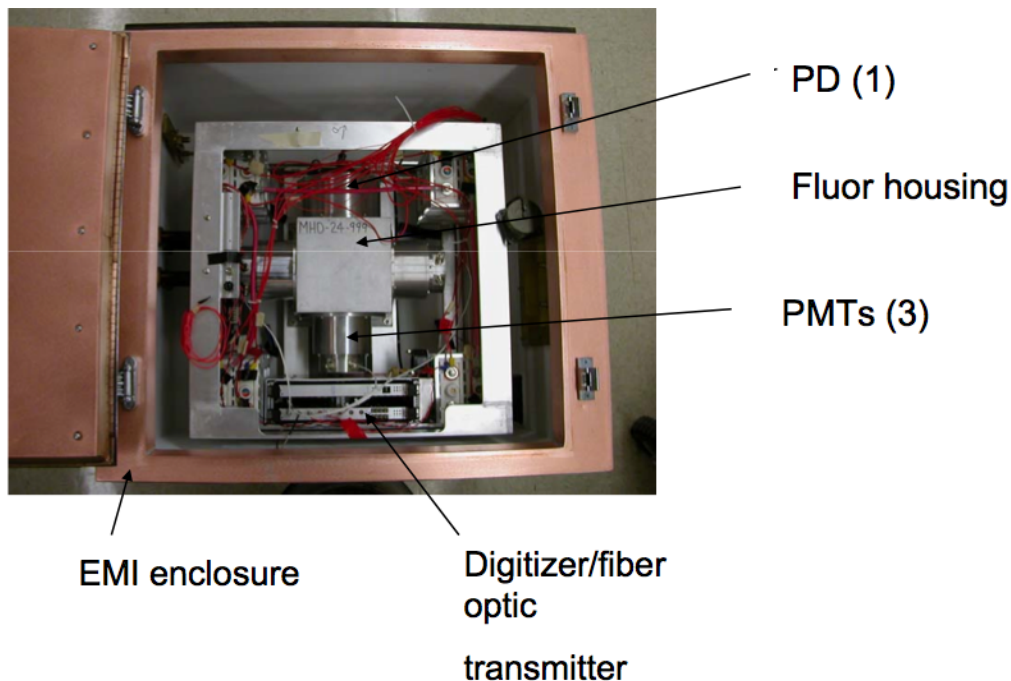
An alpha box has been developed, tested, and maintained by the Test Rediness Program. This detector is available for use at Godiva and Juliet on loan. The detector is essentially a modern version of UGT diagnostics where modern fast electronics has been located with the scintillator and photodetectors in a single housing. The housing is heavily shielded and provides mitigation of emf. Neutron and gamma radiation cause scintillations which are detected by 4 detectors of different gains, typically 3 PMTs and 1 PD. For higher flux levels, one or more PMTs can be replaced by PDs. Given the different sensitivities, a very large dynamic range is possible. Detector coverage and output from two alpha boxes at a recent test at the Z-machine at Sandia are provided below (1" Pb shielding used for actual shot data).

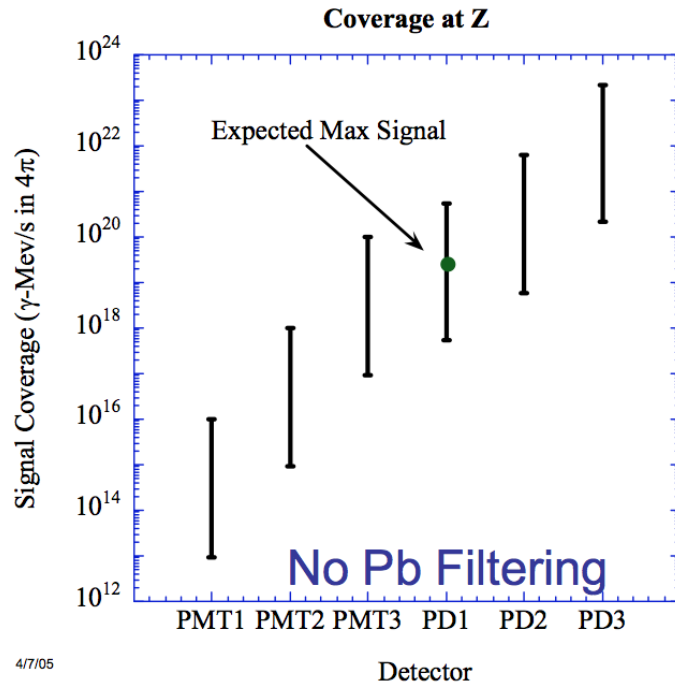
Advantages

- Already available
- Large dynamic range (over 7 orders of magnitude)
- Shielded for emf

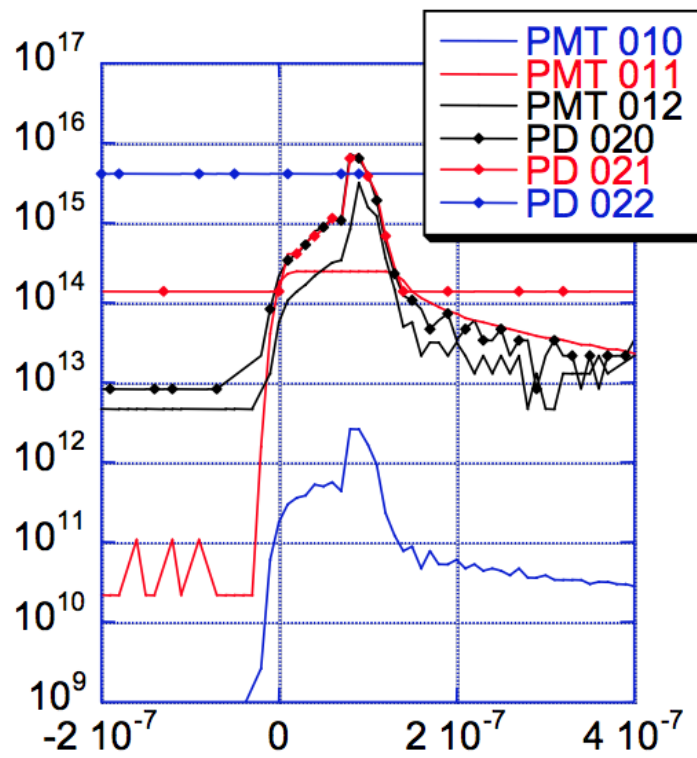
Disadvantages

- Sensitive to both neutrons and gammas
- Shielding or large stand off distance may be needed





4/7/05



CR-39 Film Pack

CR-39 film can be used to detect the integrated neutron flux. The film medium itself provides H targets for neutron scattering and a separate “proton radiator”, such as a thin poly sheet, typically used in other methods based on proton recoil, is not needed. The damage to the film medium caused by the recoils can be chemically etched to produce optically measurable holes in the film, the density of which is proportional to the integrated neutron flux.

Frenje (Rev. Sci. Instrum., 73, 2002) describes the use of a stack of 4 CR-39 films, with aluminum ranging filters (100 μm) between and outside, to measure 2.45 MeV neutrons from DD fusion. The Al ranging filters prevent protons from reaching adjacent films. The CR-39 stack was located 15 cm from the DD source with a total neutron yield of 1.3×10^{11} . The dynamic range may be extendable, as discussed in the ref., to $10^{12} - 10^{13}$ n with non-linear corrections for track overlap. The measured detector characteristics are provided below.

CR-39 film is used at LLNL in dosimetry applications as well as for calibration of detectors at NIF. The etching and optical reader hardware as well as the necessary experience and proficiency in CR-39 film reading already exist at LLNL.

Sensitivity: 1.1×10^{-4} etched tracks/n

Dynamic Range: $3.5 \times 10^6 - 3.5 \times 10^{10}$ n/cm² with linear response

Advantages

- Preferred in high flux conditions to other film/track detectors
- Large dynamic range (may be extendable to $10^{12} - 10^{13}$ n)
- Insensitive to gammas
- Well established technique and available at LLNL

Disadvantages

- Improper chemical etching could result in systematic errors.

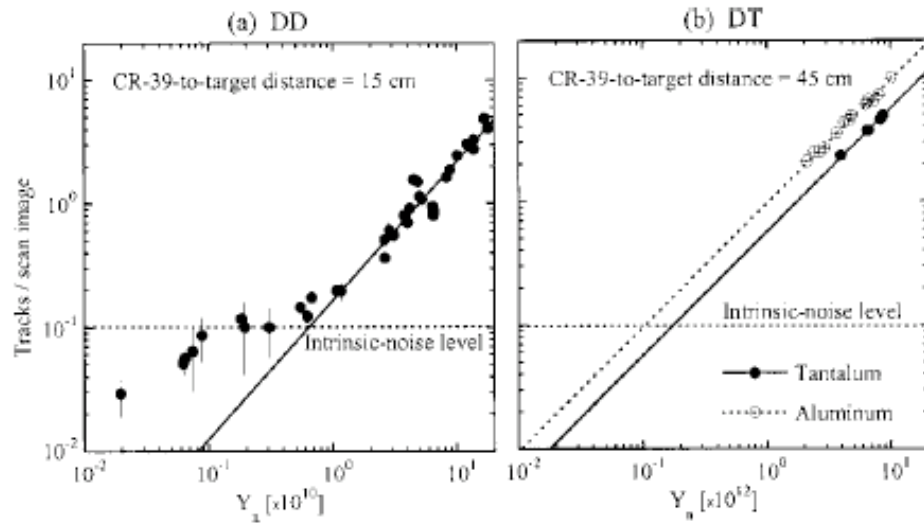


FIG. 12. (a) Number of DD-neutron-induced tracks (within the diameter range 6–12 μm) per scan image ($1.3 \times 10^{-3} \text{cm}^2$) as a function of implosion yield (where the yield was measured with either indium activation or a neutron time-of-flight diagnostic). The data were extracted from the front sides of the CR-39 using scan parameters (85/65/15). The CR-39 detectors were located 15 cm from the target in all cases. The solid line indicates a linear fit to the data above a neutron yield of 10^{10} , indicating that useful yield estimates can be made in that regime. Intrinsic noise, nominally indicated by the horizontal dotted line, dominates at lower yields. (b) Number of DT-neutron-induced tracks (within the diameter range 6–12 μm) per scan image is plotted as a function of DT neutron yield determined from copper activation. The data were acquired using aluminum or tantalum filters in front of the CR-39. The CR-39 pieces were located 45–60 cm from the targets, but all data are normalized to 45 cm by correcting for R^{-2} and for backscatter effects. It can be seen that the aluminum filter acts as an external charged-particle source and increases the number of neutron-induced tracks by about 60% in the CR-39 (relative to tantalum). The DT data show a strong linear correlation between track density and neutron yield, and extrapolation to lower neutron yield indicates that at 15 cm from the target the method should work down to at least 10^{10} , where intrinsic noise would start to dominate. There is an upper limit on yield for this method of about 10^{14} , where track overlap in the CR-39 starts to be significant.

Activation and RadChem Foils

Activation foils have been used extensively to characterize radiation fields at pulsed reactors and other high radiation environments. Integrated neutron fluence at several location within and external to the assembly can be measured with the foils. Different foil materials and shields can be used to grossly measure the neutron energy spectrum. Recently, Kelly (IEEE Trans. Nuc. Sci., V40, 6, 1993) used foils to benchmark Sandia's SPR-III pulsed reactor neutron spectrum inside the cavity. A large number of activation materials over a number of separate pulses were used (see Table below). The activation of the foils, in conjunction with Monte Carlo modeling and in-house software, was used to deduce the neutron spectrum. The best and minimum set of foils for application to Juliet has not been determined as of yet.

Advantages

- Usable in high flux conditions
- Insensitive to gammas
- Well established technique

Disadvantages

- Software needed for spectrum determination
- Time lag between foil retrieval and measurement could reduce accuracy
- Impurities in materials needs to be known and/or pure materials procured.

TABLE 3: 31°K III SENSOR ACTIVITIES

Sensor Reaction	Foil® Cover	Shot	Measured Activity (Bq/nucleus) ^a	MCNP Calculated C/E Ratio	Stat. Tests Passed	SAND-II Unfold C/E Ratio	Measured-to- Cat. Dev. (%)	ΔC _{95%} (%)	95% Energy Response Limits Lower Upper
1* 197Au(n,γ)198Au	Cd	8869	6.574E-18	4.5	6/10	1.0269	-2.621	0.886	4.750E-6 1.700E+0
2* 197Au(n,γ)198Au		8869	7.414E-18	4.5	6/10	0.9766	2.410	0.836	8.800E-8 1.600E+0
3* 59Co(n,γ)60Co	Cd	8843	6.923E-22	2.9	7/10	0.9747	2.568	3.58	1.150E-4 1.700E+0
4* 63Cu(n,γ)64Cu	Cd	8843	3.302E-18	2.2	9/10	1.0266	-2.585	15.4	2.100E-2 2.400E+0
5* 115In(n,n')115mIn		8827	6.204E-17	4.7	10/10	0.9766	2.350	2.60	1.000E+1 5.900E+0
6* NaTi(n,X)46Sc	Cd	8843	7.325E-21	3.4	10/10	0.9524	5.009	4.51	3.800E+0 7.300E+0
7* NaTi(n,p)47Sc	Cd	8843	2.882E-19	2.7	10/10	1.0673	-6.314	6.20	1.700E+0 7.500E+0
8* 48Ti(n,p)48Sc	Cd	8843	8.684E-21	1.2	8/10	0.9443	5.869	4.04	5.900E+0 1.230E+1
9* 32S(n,p)32P*		8843	2.508E-19	3.0	10/10	1.0050	-0.486	19.41	2.300E+0 7.200E+0
10* 58Ni(n,p)58Co	Cd	8827	8.752E-20	3.1	10/10	0.9662	3.462	4.49	2.000E+0 7.400E+0
11* 54Fe(n,p)54Mn	Cd	8843	1.400E-20	3.2	8/10	1.0331	-3.197	3.05	2.300E+0 7.400E+0
12* 56Fe(n,p)56Mn	Cd	8843	5.408E-19	2.4	8/10	1.0097	-0.956	4.30	5.500E+1 1.120E+1
13 64Zn(n,p)64Cu	Cd	8843	3.882E-18	2.2	8/10	1.0452	-4.323	7.41	2.400E+0 7.400E+1
14* 24Mg(n,p)24Na	Cd	8827	1.242E-19	3.0	8/10	1.0648	-6.086	3.72	6.500E+0 1.160E+1
15* 27Al(n,α)24Na	Cd	8827	6.135E-20	1.9	8/10	0.9940	0.561	2.61	6.400E+0 1.200E+1
16* 90Zr(n,2n)89Zr	Cd	8843	1.616E-21	3.4	5/10	1.0016	-0.161	2.72	1.270E+0 1.750E+1
17* 235U(n,f)140La	Tcd	8835	1.755E-11	3.0	8/10	0.9872	1.280	0.457	6.300E-2 4.100E+0
18* RMLEU	B4C, Tcd	8894	1.500E-11	3.3	8/10	0.9872	1.266	0.457	8.000E-2 4.200E+0
19* 239Pu(n,f)140La	Tcd	8835	2.317E-12	3.2	8/10	0.9747	2.624	0.644	1.500E+0 6.600E+0
20* RMLDU	B4C, Tcd	8894	2.223E-12	3.2	8/10	0.9833	1.718	0.638	1.400E+0 6.600E+0
21* 239Pu(n,f)140La	Tcd	8835	2.233E-11	2.7	10/10	1.0377	-3.633	2.97	8.800E-2 4.300E+0
22* RMLPU	B4C, Cd	8894	1.912E-11	3.2	10/10	1.0524	-4.979	2.82	1.100E-1 4.500E+0
23* 237Np(n,f)140La	Tcd	8835	1.234E-11	2.8	10/10	0.9709	3.039	10.32	5.250E-1 5.300E+0
24* 237Np(n,f)140La	B4C, Tcd	8835	1.182E-11	2.8	10/10	0.9690	3.183	10.31	5.250E-1 5.300E+0
25 45Sc(n,γ)46Sc	B4C, Tcd	8835	1.192E-20	3.5	9/10	----	----	5.29	3.200E-2 1.500E+0
26 45Sc(n,γ)46Sc	Cd	8827	1.372E-20	3.3	9/10	----	----	5.13	1.425E-2 1.400E+0
27 23Na(n,γ)24Na	B4C, Tcd	8835	5.963E-20	2.1	7/10	----	----	17.70	5.000E-2 2.800E+0
28 23Na(n,γ)24Na	Tcd	8827	7.170E-20	2.1	9/10	----	----	17.41	3.400E-2 2.700E+0
29 55Mn(n,γ)56Mn	B4C, Tcd	8835	4.557E-18	2.7	8/10	----	----	17.65	2.700E-2 2.400E+0
30 55Mn(n,γ)56Mn	Cd	8827	6.618E-18	2.6	6/10	----	----	17.48	3.200E-4 2.100E+0
31 58Fe(n,γ)59Fe	Cd	8869	7.974E-21	2.8	10/10	----	----	29.92	1.900E-2 2.300E+0
32 27Al(n,p)27Mg	Cd	8827	2.872E-17	3.0	8/10	----	----	10.83	3.500E+0 9.200E+0
33 115In(n,γ)115mIn	Cd	8827	4.916E-16	1.3	7/10	----	----	6.17	1.425E-6 2.100E+0
34 23Na(n,γ)24Na		8827	7.087E-20	2.1	8/10	----	----	15.55	3.200E-8 2.500E+0

© Cover composition: 91.67% 10B-enriched B4C=0.1481 atoms/barn; Cd=2.567E-3 atoms/barn; Tcd=4.705E-3 atoms/barn of Cd

* Assume the use of the 1993 GLUCS 32S(n,p)32P cross section, MAT=1625. This is consistent with use of the SNL-RM, cross section library.

§ Fission foil activities are in units of reactions/nucleus

Time of Flight

The Advanced Detector Design Group at LLNL has provided a preliminary design for a TOF spectrometer. The TOF detector in conjunction with a ^3He ionization tube can provide spectral coverage for neutron energies from a few keV to over 10 MeV. The spectrometer consists of two scintillators with a 1 m long drift tube between them. The time difference measured between interactions of individual neutrons in the front and back scintillators provides a very accurate energy measurement to within a few %. A liquid scintillator in the front can allow for gamma discrimination via pulse shape analysis. Accuracy begins to diminish to 20% below several hundred keV where a ^3He ionization tube is then used to improve accuracy.

Advantages

- Most accurate neutron energy measurement method
- Relatively simple hardware and electronics required

Disadvantages

- Usable only in low flux conditions (necessary for single neutron counting)
- Measures neutrons only in a specific direction
- Relatively large and heavy

Ionization Tube

^3He ionization tubes can be used to measure the neutron energy spectrum below a few 100 KeVs. Ionization of the gas by protons from the $^3\text{He}(n,p)\text{T}$ reaction causes electron cascades in the tube resulting in pulses. The pulse amplitude can provide information relative to the incident neutron energy. A significant drawback is the complex defolding of the pulse height spectra to determine neutron energy (see e.g. Matysiak W., Nuc. Instrum. Meth, A, 592, 2008).

Advantages

- Well known technique
- Relatively simple hardware and electronics required
- Measures neutrons from all directions with relatively high sensitivity

Disadvantages

- Requires software and complex algorithms to deduce neutron spectrum.

Neutron Trap

LLNL B-division has fielded a simple detector consisting of a large 1 ft³ of plastic scintillator coupled to a PMT. Long after the pulse from the reactor is over, some neutrons continue to scatter at thermal temperatures for long time periods of up to msecs. By gating the signal from the PMT, only capture gammas from neutron capture by protons provide a signal at long times. The detected number of gammas is related to the total neutron yield of the pulse. This detector was successfully fielded on Full Toss but would need to be fully calibrated for Godiva and Juliet use with respect to room return signatures at delayed fission gammas and neutrons which also occur at late times.

VISAR/PDV

VISAR (Velocity Interferometry System for Any Reflectors) and PDV (Photonic Doppler Velocimeter) are interferometry techniques which allow the measurement of complete time histories of the motion of a surface for very fast reaction times, such as shocks. Crump (SAND92-0162) describes a modification to the basic technique, known as Fixed Cavity VISAR, which allows the triggering of recording equipment on the initial motion of the measured object. This would be appropriate given the imprecise knowledge of the reaction and shock generation in the Godiva or Juliet assemblies.

The primary components of a typical VISAR set-up are a single frequency laser, modified unequal leg Michelson interferometer cavity, high-speed PMTs, and a digitizing oscilloscope. A sketch of a Fixed Cavity VISAR is provided below with description of operation provided in the reference. A typical data output from a multipoint VISAR is also shown below.

Both VISAR and PDV have been used extensively for subcritical and hydro tests.

Advantages

- Usable in high EMF conditions
- Not sensitive to ionizing radiation
- Well known/used technique at LLNL
- Portable PDV module already developed and available

Disadvantages

- VISAR and PDV if built from scratch are expensive.

Retroreflective Shadowgraphy

Retroreflective shadowgraphy is an old visual technique developed by Edgerton. A simple set-up includes a light source (arc lamp), fast camera ($>250,000$ fps), and retroreflective screen (commercially available). This technique has been used to visualize explosive shocks in air as well as many other dynamic events causing refractive index changes in air (Hargather 2009). Diagrams and pictures of a typical shadowgraphy setup and results are shown below.

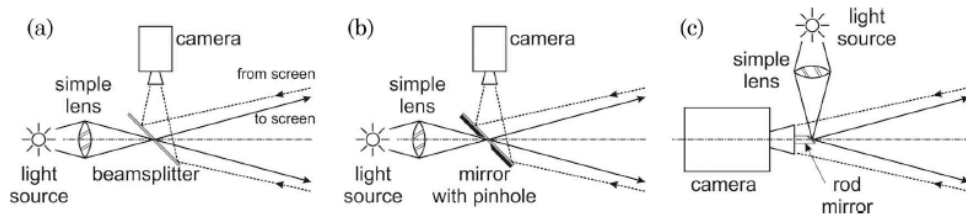


Fig. 3. Diagrams of the coincident illumination setups for retroreflective shadowgraphy, using (a) a beam splitter, (b) a mirror with a "pinhole," and (c) a rod mirror.

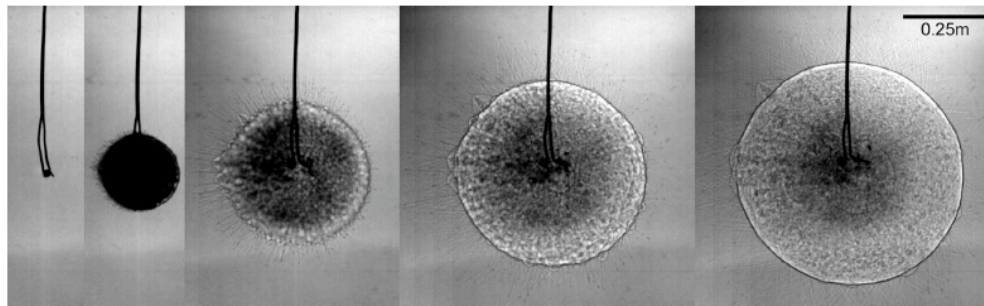


Fig. 5. Digital image series showing shadowgrams of a 1 g TATP explosion.

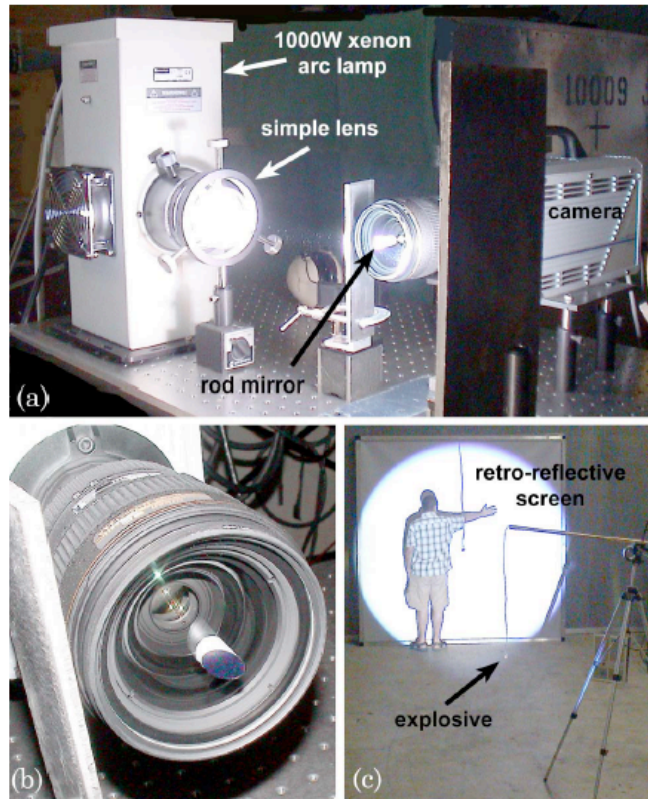


Fig. 4. (Color online) (a) Oblique side view of the camera/illuminator assembly, with vertical plates used as beam stops. (b) APX-RS digital camera with a 20–70 mm Nikon zoom lens and the rod mirror mounted on a clear lens filter. (c) An explosive charge is suspended by a wire in the foreground while the author (MJH) stands before the retroreflective screen in the background, on which the shadowgram of the suspended charge can be observed.